Experimental study of the effect of internal pressure on oscillating behavior of pool fires

Jian Chen[1], Wai Cheong Tam[2], Wei Tang[2], Chao Zhang[2], Changhai Li[1], Shouxiang Lu[1,*]

[1] State Key Laboratory of Fire Science, University of Science and Technology of China, Hefei 230026, China

[2] Fire Research Division, National Institute of Standards and Technology, MD 20899, United States

[*] Corresponding author: Prof. Lu Shouxiang; E-mail: sxlu@ustc.edu.cn

Abstract

A series of experiments have been conducted to study the flame behavior of ethanol pool fires in a closed chamber. The effect of internal pressure and the size of the pool burner is considered. Tests include pressure conditions ranging from 50 kPa to 350 kPa and 5 circular pool burners with different diameters (2 cm, 4 cm, 6 cm, 8 cm, and 10 cm). Measurements such as gas temperature, internal pressure, oxygen concentration, and video record for all tests are obtained. Steady-state burning period is identified to facilitate a quantitative analysis of flame behavior. Image processing is carried out to obtain time average appearance of pool fires. The concept of oscillation intensity is introduced. Oscillation behaviors of pool fires in a closed system as a function of internal pressure and pan diameter are correlated with oscillation intensity. Four flame structures are observed: laminar, tip flicking, sinuous meandering, and turbulent flame. Relationships between oscillation intensity to flame structure and Grashof number to flame structure are established. Effect of internal pressure and gravitational force to oscillation frequency is also accessed. Simple theoretical model is developed. An empirical expression using the relationship of Strouhal number and Grashof number is established. Two distinct behaviors on oscillation frequency as a function of pressure are observed.

Results obtained from this work will facilitate the understanding of oscillation behavior of ethanol pool fires in different sizes with various internal pressure conditions in a closed chamber.

Keywords

Pool fire; Internal pressure effect; Flame structure; Oscillation frequency

Nomenclature

a	acceleration induced by buoyancy	ΔT	temperature difference between flame and ambient temperature
d	diameter of pan	T_f	flame temperature
c_p	the heat capacity of air	T_∞	ambient temperature
f	oscillation frequency	u	velocity components along x
Fr	Froud number	u_0	characteristic velocity
g	gravitational acceleration	v	velocity components along y
Gr	Grashof number	v^*	characteristic velocity of the vortex
I	oscillation intensity of pool fire		
l^*	characteristic length of the vortex	V	flame volume
l	characteristic length		*Greek symbols*
P	internal pressure	ν	kinematic viscosity
$\dot{Q}$	heat release rate	μ	dynamic viscosity
R	universal gas constant	ρ	gas density
Re	Reynolds number	ρ_∞	air density
Ri	Richardson number	$\Delta\rho$	density difference
St	Strouhal number	β	the thermal expansion coefficient of the air
t_{conv}	convection time		

1. Introduction

The study of buoyant diffusion flame (i.e. pool fire) is one of the most important areas in fire research community as it provides the fundamental understanding about the complex interactions between the fluid dynamics and the chemistry. Under normal atmospheric conditions, a significant amount of research efforts have been made, for example, through means of experiments [1-4], scale

modeling [5] and numerical simulations [6, 7]. Numerous experiments [1-4] over the past several decades have shown that the flame oscillation frequency could be well correlated with the square root of the burner diameter or the fourth root of the burner surface area. The applicability of this relationship is truly remarkable considering a wide range of pool diameters from 0.01 m to 1 m with different fuel types such as spanning solid fuels, liquids and gaseous fuels including polymethyl methacrylate, methanol, ethanol, acetone, crude oil, hydrogen and methane [2]. It was observed that the periodic behavior of pool fire is not a result of combustion chemical reaction, but rather the flow of free convection. Moreover, it was also noticed that the oscillation behavior of pool fire does not occur when the burner diameter or the fuel velocity is below a critical value [1, 7].

Based on dimensional analysis, the important effect associated with different driving forces on the oscillating behavior was investigated [1, 2, 5]. Emori and Saito [5] introduced the Strouhal (*St*) number and Froude (*Fr*) number to explain the change of oscillation frequency where the burner diameter was deemed as the characteristic length in the calculation of dimensionless numbers. Hamins et al. [1] measured the pool fire frequency over a wide range of burner diameter from 0.0074 m to 0.30 m and they found that the dimensionless oscillation frequency expressed by *St* number is proportional to the -0.57 power of *Fr* number over 14 orders of magnitude in *Fr* number. Cetegen et al. [2] also has proposed the equation of pool fire pulsation frequency using the Richardson (*Ri*) number. Here, it should be noted that the *Fr* number is equal to the inverse of *Ri* number mathematically. The above studies confirmed the importance of pool diameter and gravity on the pool fire oscillating behavior and both scaling studies determined that $f \sim d^{-1/2}$ which is in general accord with the experimental measurements.

These studies under atmospheric conditions have deepened the understanding of pool fire oscillation mechanisms and suggested that the flame oscillation is caused by the instability of buoyancy flow. The buoyant force of hot gas can be expressed as $\Delta\rho gV$ where $\Delta\rho$ is the density

difference between ambient air and flame, and g is gravitational acceleration. The buoyant force is linearly dependent on $\Delta\rho$ and gravity, so the ambient pressure and gravity have significant influence on the oscillating behavior. Abe et al. [8] used a high-speed camera to record the oscillating behavior of small-scale pool fires with diameters from 1 cm to 3 cm under low-gravity environment. It was found that when the gravitational acceleration decreased, the oscillation of the pool fire was suppressed. Yuan et al. [9] carried out methane jet diffusion flames with burner diameters ranging from 0.22 cm to 0.4 cm under different pressures and gravity and found that the decrease of pressure also could suppress flame oscillation. The measured results showed the flickering frequency is proportional to the 2/3 power of the gravity, and 1/3 power of the pressure. Besides, the similar relationship between frequency and pressure were also found and verified in small scale ethanol pool fire in the recent study [10].

Considering its controllability and convenience, available experimental data on flame oscillation under reduced or high pressure is limited to small scale pool fire where the diameter is in the range of 0.22 cm and 3 cm [8-10]. Generally, most of the combustion in industrial applications is turbulent combustion which involves larger-scale pool fire than laboratory scale. However, nearly no work has been done to understand the influence of high pressure on the oscillating behavior of larger scale pool fires. As mentioned in the above research under normal pressure [1, 2], the diameter of a pool fire has proven to be an important factor in its oscillating behavior. The flame oscillation behavior was then controlled by the coupling of diameter and pressure. As the pool diameter increases, it is not certain if the existing relationship remains applicable or whether another oscillation mechanism would be discovered is still unknown. In summary, considering the combined effect of pressure and diameter, a global model for the prediction of flame structure and oscillation frequency should be built.

To fill these knowledge gaps, the effect of ambient pressure on the pool fire with different scale range from 2 cm to 10 cm is considered in this work. The paper is broken into several parts. In

the section of experiment, ethanol pool fires with different diameters were conducted under different pressure conditions ranging from 60 to 250 kPa, where pressure conditions were attained and maintained using a high-pressure chamber. In order to minimize the enclosure effects of pressure chamber, the thermal parameters were measured and the relative stable stage was selected where the change of thermal properties of air in the chamber were controlled within a certain range. The experimental and calculated results reported later were limited to those obtained in the relative stable stage. In the section of results and discussion, the dimensional analysis was performed to explain the flame structure changing from laminar to turbulent, and a mathematical method was introduced to quantify the oscillation intensity of pool fire. In addition, based on the one-dimensional movement of vortex along the axis, the empirical correlation of oscillation frequency was validated using data in our and previous studies. The results are summarized in Section 3.

The main contribution of this study is to better understand the flame oscillation behavior. The division for flame structure and the established model for flame oscillation frequency can provide a scientific prediction for the complex structure of buoyancy diffusion flame. Another object of this study is to enrich the experimental results of pool fire with larger scale under different ambient pressure which is useful in the development of combustion model.

2. Experiment

2.1 Experimental setting

Experiments are conducted using an in-house experimental platform. Although the details associated with the experimental setup are described in reference [10], significant details are provided below to help readers to understand the experiment. As shown in Fig. 1, the experimental platform is consisted of 4 primary components: 1) a closed chamber, 2) a pressure control system, 3) a data acquisition system, and 4) a pool burner. The chamber is constructed using 304 L stainless

steel. It has nominal internal dimensions of 0.6 m in height and 0.4 m in diameter. The thickness of the stainless-steel bounding surfaces is about 5 mm. There are two circular openings on the chamber and they are located opposite to each other. The dimension of the openings is identical and is about 12 cm in diameter. High temperature tempered glazing is used. Home-grade sealer is applied to avoid air leakage.

The pool burners are all circular and are made of steel. In this work, there are 5 burners with different diameters (2 cm, 4 cm, 6 cm, 8 cm, and 10 cm). Each burner has a nominal depth of 2.5 cm and the rim thickness is about 0.2 cm. The purpose of the burner is to contain fuel and ethanol (C_2H_5OH) is selected for the study. Previous studies [12, 13] showed that lip height, the distance between the top of burner and the fuel surface, is an important factor for liquid pool fire experiments [11]. For that, the initial lip height for all experiments is controlled to be 0.15 times of the burner diameter of burner and its fluctuation is maintained to be less than 5 %.

The pressure control system has two parts: a vacuum pump and a pressure pump. Using this setup, an initial target pressure in the chamber can be achieved. There are two different pressure conditions in our experiments. For reduced pressure conditions, a vacuum pump is used. For high pressure conditions, the pressure pump is used to supply air to the chamber. It should be noted that the pressure control system only provided the initial target pressure for the chamber and the actual pressure reading varies over time during a pool fire burn. In general, the pressure increases during the burn and safety valve is installed on the top of the pressure chamber to prevent pressure exceeding the intended maximum pressure conditions.

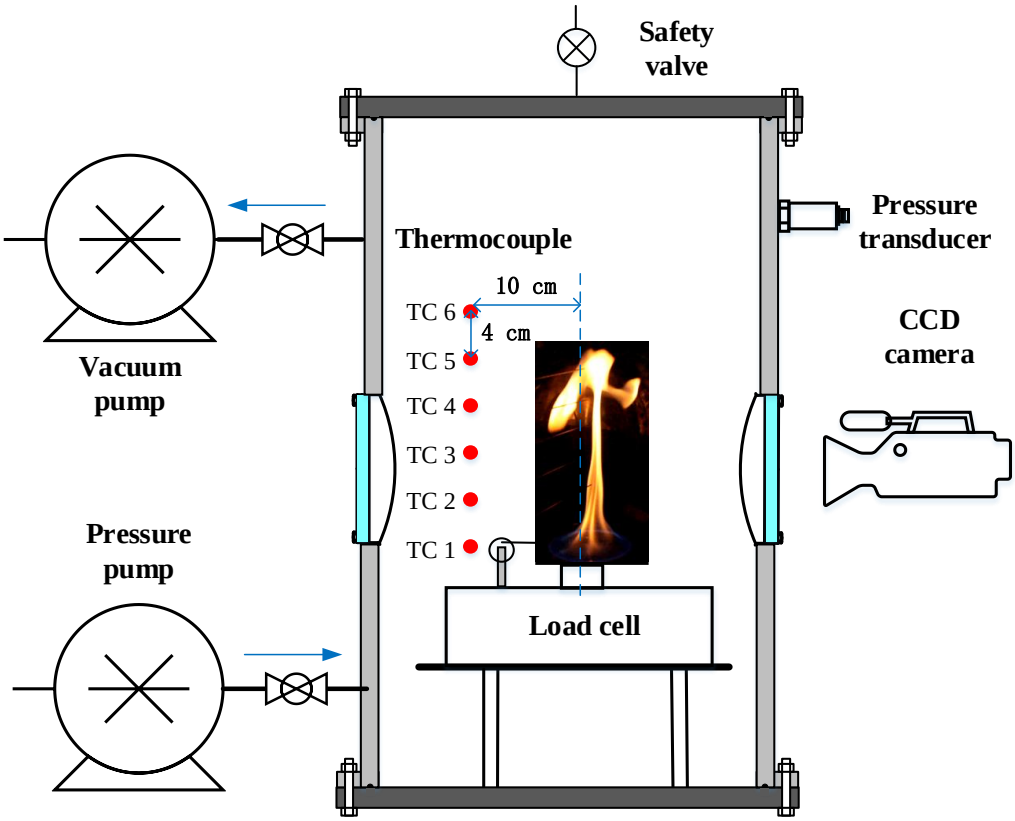

Fig. 1. Schematic of experimental platform.

The data acquisition system is capable to obtain video record of pool fire, mass loss rate of the fuel, gas temperature at different locations, and pressure in the chamber. A CCD camera is used to record video data of the pool fires. The camera is located outside of a window opening. Angle of the camera is adjusted to accommodate video recording of different runs. The camera has a resolution of 1280 × 720 in pixels with 60 frames per second. Other settings of the camera are in default. Two different load scales[1] are used separately for the experiments and they are the Mettler Toledo WKC603C with a measuring range of 620 g with resolution of 1 mg and the Mettler Toledo

[1] Certain commercial equipment, instruments, or materials are identified in this paper in order to specify the procedures adequately. Such identification is not intended to imply recommendation or endorsement by the National Institute of Standards and Technology, nor is it intended to imply that the materials or equipment identified are necessarily the best available for the purpose.

WKC6002C with a measuring range of 6200 g and resolution of 10 mg. The purpose of using different load scales is to facilitate proper weight measurement of fuel for burners with different diameters. K-type thermocouples with a bead diameter of approximately 1 mm are used to obtain temperature measurement. As shown in Fig. 1, an array of thermocouples (labeled as TC 1 to TC 6 from top to bottom) are mounted about 10 cm away from the center of the chamber. The thermocouples are placed approximately 4 cm away from each other in vertical direction [11] where lowest thermocouple is leveled with the upper rim of the burner. A pressure transducer is located on the side of the chamber and it records the changes of pressure during the burn. The pressure gauge has a measurement range of – 60 kPa to 360 kPa and an accuracy of 2.5 % for the entire range of measurement as specified from the manufacturer.

Table 1 provides a summary of the test matrix. It can be seen that experiments are conducted using burners with 5 different diameter and in a wide range of pressure conditions in between 60 kPa and 300 kPa. It should be noted that the internal pressure increases during a burn. In order to maintain the maximum pressure during the test not exceeding 350 kPa, the maximum initial pressure condition is limited to 200 kPa and 150 kPa for 8 cm and 10 cm pool burner, respectively.

Table 1 Summary of the initial experimental conditions

Diameter (cm)	Initial fuel mass (g)	Initial pressure (kPa)
2	-	60, 80, 100, 150, 200, 250, 300
4	18.83	60, 80, 100, 150, 200, 250, 300
6	35.68	60, 80, 100, 150, 200, 250, 300
8	51.53	60, 80, 100, 150, 200
10	61.94	60, 80, 100, 150

2.2 Identification of steady state burning period

In this subsection, descriptions for experimental procedure will first be provided and then the details for the identification of steady state burning period will be given. For all tests, the experimental procedure is identical and it involves four steps: 1) the pool burner is placed onto the load scale in the chamber. Fuel is added and the net weight of fuel is measured. In order to avoid

excessive fuel evaporation before ignition, the burner is covered by an asbestos board; 2) once the pool burner is settled, the pressure chamber is closed and the pressured control system is turned on. Once the initial target pressure condition is reached, we wait about 5 minutes to ensure no leakage; 3) before ignition, the asbestos board is removed by a pre-programed servo system. A 2.5 mm diameter Ni-Cr wire is used to ignition the fuel; 4) in all experiments, the pool fire is self-extinguished in the chamber and it happens when the oxygen concentration decreases to a certain level. Once the pool fire is extinguished, measurement is made for the oxygen concentration and it is assumed that the gas in the chamber is well mixed. Measurements (gas temperature, oxygen concentration, burning rate, pressure, and videos) are obtained using the data acquisition system. Each test is repeated 2-3 times to ensure repeatability.

It is well understood that gas temperature, oxygen concentration, burning rate, and pressure will continuously be changing during the test. Some of these measurements are observed to have completely different behaviors at various fire growth stages. Comparison between tests and studies associated with the fire dynamics and flame behavior are relatively difficult to be conducted. For that, a steady state burning period is needed to be identified.

Fig. 2 shows the measurements for an ethanol pool fire experiment using a 4 cm diameter burner with an initial pressure condition at 200 kPa. It can be seen that oxygen concentration decreases linearly whereas the chamber pressure, burning rate, and gas temperature undergo 3 distinct stages: a rapid increase stage, a developed stage, and a rapid decrease stage. During the developed stage, the value associated with the pressure, burning rate, and gas temperature increase rather slowly. As shown in the figure, the changes associated with pressure, burning rate, and temperature are less than 5 %. With that, measurements in between the dimensionless/normalized time in between 2/5 to 3/5 are selected for further analysis. Moreover, the oxygen concentration in the range of 19 % to 16 % and based on reference [14], this limiting condition has relatively minor influence on the pool fire flame. It is worth noting that the dimensionless time is used to

accommodate the difference in burn duration for each test.

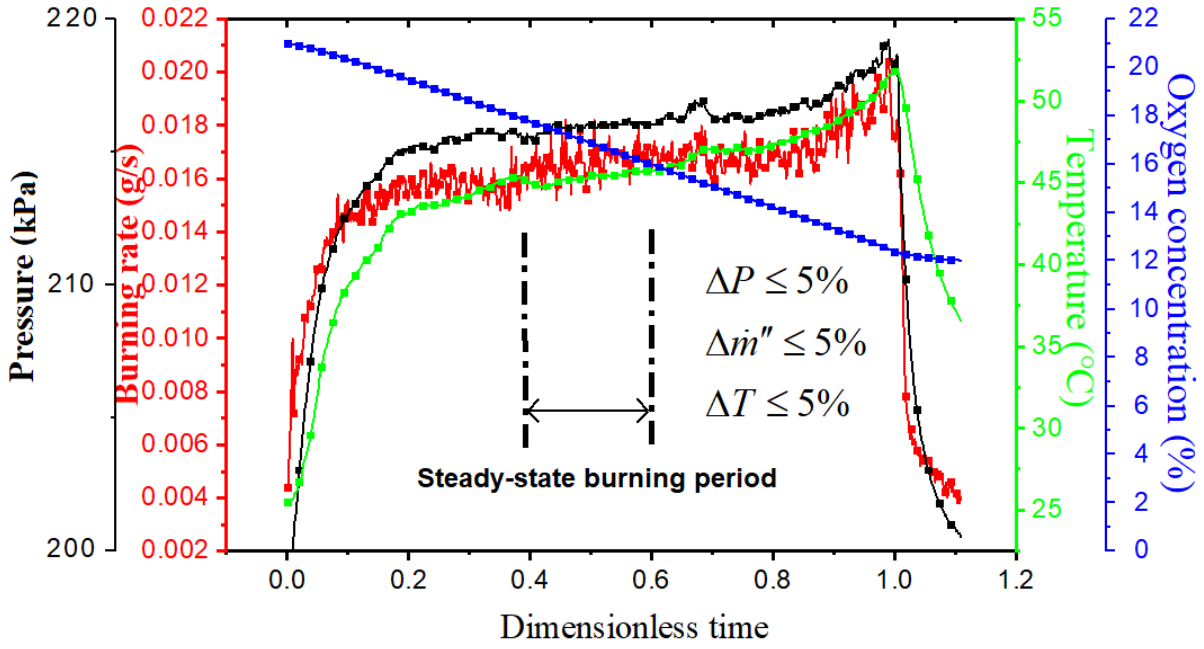

Fig. 2. Measurements associated with ethanol pool fire experiment using a 4 cm diameter burner with initial pressure condition at 200 kPa.

3. Results and discussion

3.1 Flame structure

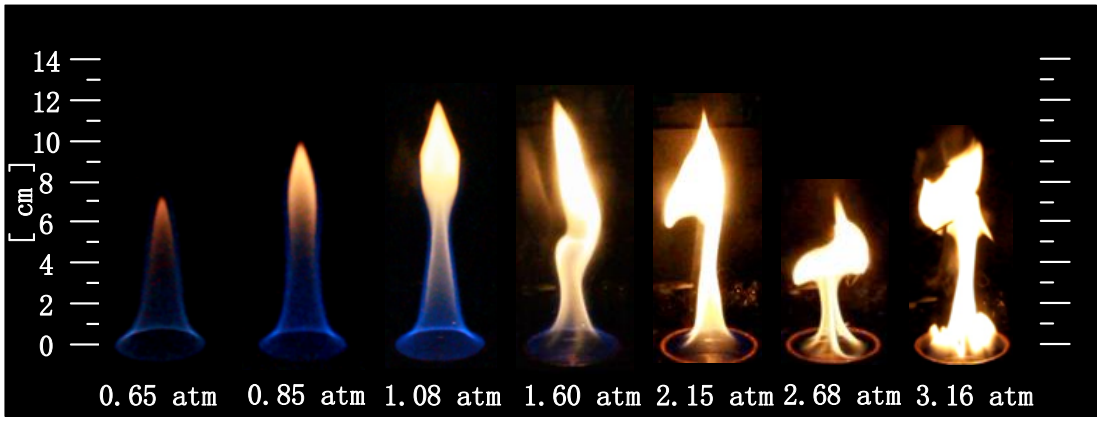

Fig. 3. Flame appearance of ethanol pool fire with 4 cm diameter for different pressure conditions.

Fig. 3 shows images of ethanol pool fires with 4 cm diameter burner at different pressure conditions. It can be seen that the pressure has strong effect to the flame appearance. At reduced

pressures (i.e. 65 kPa and 85 kPa), the flame color appears to be mostly blue. As the pressure increases, the blue region of the flame shrinks and the flame becomes yellow. It is believed that the change in color of the flame can be explained by the difference in chemical reactions associated with different pressure conditions [15]. When the pressure is low, radicals existed in the pool fire are typically C_2 and CH [15, 16]. For that, the flame color appears to be blue. However, as the pressure increases, the formation time of soot reduces and the oxidation time of soot increases [16]. With that, more soot particulates are generated within the flame. Therefore, the flame becomes yellow. It is also noticed that, with the increase in pressure condition, the flame becomes unstable. The flame tip starts to oscillate and wrinkled corrugations appear on the flame envelop. Similar observation is found in experiments with burners in different diameters. For a given pressure, more violent oscillations are observed for pool fires with larger pool diameter. In order to better understand the relationship between the burner diameter and the pressure condition to the flame oscillation, dimensional analysis is conducted.

Pool fire is a type of diffusion flames driven mainly by buoyancy force. The gas movement is induced by the temperature gradient between the flame boundary and the ambient fluid. In our analysis, it is assumed that the flow is incompressible, two-dimensional, and in steady state. Thermal properties of the fluid are treated to be constant [17]. With that, the governing equation can be expressed as:

$$u\frac{\partial u}{\partial x}+v\frac{\partial u}{\partial y}=g(\Delta\rho/\rho)+\nu\frac{\partial^2 u}{\partial y^2} \tag{1}$$

where u is velocity in x-direction, v is the velocity in y-direction, g is the gravitational force, ρ is the density, and υ is the kinematic viscosity of ambient air. It should be noted that x-axis is perpendicular to the pool surface and y-axis is parallel to the pool surface. According to Boussinesq approximation, a volumetric expansion coefficient can be introduced:

$$\beta \approx -\frac{1}{\rho} \times \frac{\Delta\rho}{\Delta T} \tag{2}$$

Substituting Eqn. 2 into Eqn. 1, the governing equation/momentum equation is rewritten as:

$$u\frac{\partial u}{\partial x} + v\frac{\partial u}{\partial y} = g\beta(T - T_\infty) + \nu\frac{\partial^2 u}{\partial y^2} \tag{3}$$

Introducing the following dimensionless variables,

$$x^* \equiv \frac{x}{l}$$

$$y^* \equiv \frac{y}{l}$$

$$u^* \equiv \frac{u}{u_0} \tag{4}$$

$$v^* \equiv \frac{v}{u_0}$$

$$T^* \equiv \frac{T - T_\infty}{T_f - T_\infty}$$

where l is the characteristic length, T_f is the flame temperature, and T_∞ is the ambient temperature. Using the dimensionless variables suggested in Eqn. 4, Eqn. 3 becomes:

$$u^*\frac{\partial u^*}{\partial x^*} + v^*\frac{\partial u^*}{\partial y^*} = \frac{g\beta(T_f - T_\infty)l}{u_0^2}T^* + \frac{1}{\mathrm{Re}}\bullet\frac{\partial^2 u^*}{\partial y^{*2}} \tag{5}$$

where the first term in the RHS of the equation is the buoyancy force and u_0 is the characteristic velocity. In our case, since the flow is driven mainly by natural convection, the velocity is approximated as $u_0 = \sqrt{g\beta(T - T_\infty)l}$. Given that, Eqn. 5 is simplified to be:

$$u^*\frac{\partial u^*}{\partial x^*} + v^*\frac{\partial u^*}{\partial y^*} = T^* + \frac{1}{Gr^{1/2}}\bullet\frac{\partial^2 u^*}{\partial y^{*2}} \tag{6}$$

where Gr is the Grashof number which represents the ratio of the buoyancy to the viscous force acting on the fluid. Mathematically, it is given by:

$$Gr = \frac{gl^3\beta(T_f - T_\infty)}{\nu^2} \tag{7}$$

Considering the pressure effect on the kinematic viscosity, the *Gr* number can be rewritten as:

$$Gr = \frac{\left(P/RT_\infty\right)^2 gl^3}{\mu^2} \tag{8}$$

where *P*, *R*, and μ is pressure, universal gas constant, and dynamic viscosity of the air, respectively. In previous studies, the characteristic length, *l*, was taken to be the diameter of the pool. However, the previous selection of such characteristic length neglects the effect of heat release rate or the volumetric flow of the fuel [1]. In order to account for the effect of heat release rate, the following characteristic length is utilized [24]:

$$l = \left(\frac{\dot{Q}}{\rho_\infty c_p T_\infty \sqrt{g}} \right)^{2/5} \tag{9}$$

where $\dot{Q}$ is the heat release rate, c_p is the heat capacity of air at ambient temperature, and ρ_∞ is the air density. Using Eq. (9), *Gr* number becomes:

$$Gr = \frac{\left(P/RT_\infty\right)^2 g\left(\dot{Q}/\rho_\infty c_p T_\infty \sqrt{g}\right)^{6/5}}{\mu^2} \tag{10}$$

which accounts for the effects of pressure condition, diameter of pool burner, and heat release rate.

Table 2. *Gr* number and flame structure for various experimental conditions.

Gr	d (cm)	P (kPa)	T_∞ (K)	Burning rate (g/s)	Flame structure
4.53×10^5	2	60	301	0.0038	Laminar
5.67×10^5	2	80	302	0.0038	Laminar
8.24×10^5	2	100	299	0.0044	Laminar
1.43×10^6	4	65	309	0.0062	Tip flicking
2.04×10^6	4	86	310	0.0074	Tip flicking
2.11×10^6	2	200	303	0.0098	Tip flicking
2.72×10^6	4	108	313	0.011	Tip flicking
3.25×10^6	6	70	318	0.0122	Tip flicking

3.58×10^6	2	300	304	0.0134	Tip flicking
4.14×10^6	4	160	314	0.0146	Sinuous meandering
4.35×10^6	6	92	318	0.0158	Sinuous meandering
5.17×10^6	8	75	330	0.017	Sinuous meandering
5.46×10^6	6	116	322	0.0194	Sinuous meandering
5.78×10^6	4	215	315	0.0206	Sinuous meandering
6.97×10^6	10	80	333	0.0218	Sinuous meandering
7.01×10^6	8	98	323	0.023	Sinuous meandering
7.44×10^6	4	268	318	0.0242	Sinuous meandering
7.62×10^6	6	170	328	0.0254	Sinuous meandering
8.17×10^6	10	105	343	0.0266	Sinuous meandering
8.24×10^6	8	122	333	0.029	Turbulent
9.03×10^6	4	316	322	0.0302	Turbulent
1.01×10^7	6	227	329	0.0314	Turbulent
1.11×10^7	10	140	353	0.0326	Turbulent
1.14×10^7	8	186	343	0.0338	Turbulent
1.25×10^7	6	286	335	0.0362	Turbulent
1.37×10^7	10	200	363	0.0374	Turbulent
1.38×10^7	8	240	353	0.0386	Turbulent
1.50×10^7	6	340	337	0.0398	Turbulent

Table 2 shows the calculated *Gr* number and the corresponding flame structure associated with various conditions such as pressure, gas temperature, and burning rate. Fig. 4 provides a graphical representation of the flame structure for different *Gr* numbers. It can be seen that the pool fire changes from laminar flame to turbulent flame as *Gr* number increases. According to the change in flame shape and its appearance, four flame structures are identified: 1) a laminar flame in which the entire flame appears to be stable and the *Gr* number is less than approximately 1.13×10^6, 2) a tip flickering flame ($1.13 \times 10^6 < Gr < 3.58 \times 10^6$) in which the lower region of the flame is stable while the flame tip oscillates at a certain frequency, 3) a sinuous meandering flame ($3.58 \times 10^6 < Gr < 8.2 \times 10^6$) in which a pair of asymmetric vortex structures are generated near the surface of the fuel pool and develops upward movement driven by buoyancy, and 4) a turbulent flame where the *Gr* number is approximately larger than 8.2×10^6 in which the flame exhibits violently oscillation and that wrinkles can be seen on the flame envelop and clear vortices at the flame base. It is also observed

that a pair of symmetrical vortex structures convects regularly upwards from the pool surface, causing a dramatic change in flame shape.

Since the change of flame shape is a continuous process, the boundary of each flame regime is not distinct. The division of the boundaries is compared with previous studies in Fig. 4 [1, 16] where the change from laminar flame to tip flickering flame was mainly studied. Results show consistency to the order of critical values. It should be noted that the flame instability is sensitive to many factors such as experimental setup, flow conditions, and external perturbations.

In order to quantitatively describe the transition of the flame structure from laminar to turbulent, it is necessary to define a physical parameter that can correlate the oscillation intensity of a pool fire. In the field of fluid mechanic, the turbulence intensity is defined as the ratio of the root-mean-square of the velocity fluctuations to the mean flow velocity. In the study of Fang et al. [15], the oscillation intensity was defined as the ratio of half of the flame oscillating amplitude to the mean flame length. It was used to explore the effect of reduced pressure on the oscillating behavior of flickering flame. However, the flame oscillating amplitude is not constant for turbulent pool fires. Therefore, a probabilistic approach is used to characterize the oscillation intensity of pool fire.

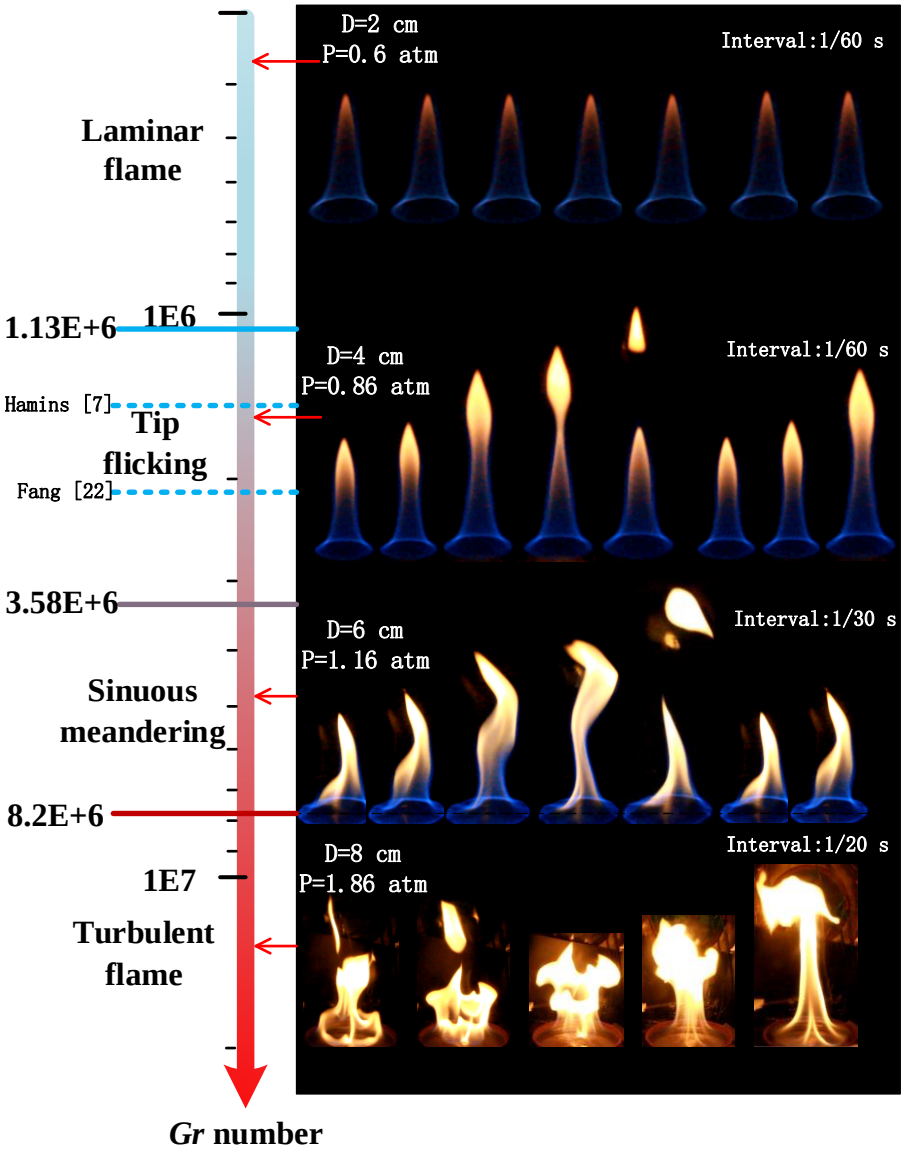

Fig. 4. The change of instantaneous flame structure with *Gr* number.

The flame videos recorded in the experiment are decompressed into RGB images. A luminance threshold suggested by Otsu [3, 19] is used to separate the region of flame and the background. Using the suggested value, the background is subtracted and RGB images are transformed into binary images. The RGB image and binary image of a same frame are shown in Fig. 5 (a) and Fig. 5 (b), respectively. By direct comparison, the overall size and shape of the flame are nearly identical.

In one experiment, approximately 3600 binary images can be obtained from the steady state burning period (refer Sec 2.2). These images represent many cycles of the pool fire that is similar to that of shown in Fig. 4. Given a binary image, the flame appearance for every pixel can be determined. Using the set of images, the probability of flame appearance is obtained. Fig. 5 (c) shows the probability contour for an ethanol pool fire with different *Gr* numbers. It should be noted that contour lines for different probability values are provided. In the figure, a value of 0.05 indicates that flame is detected 5 % out of all available images for an experiment.

(a) Original image

(b) Binary image

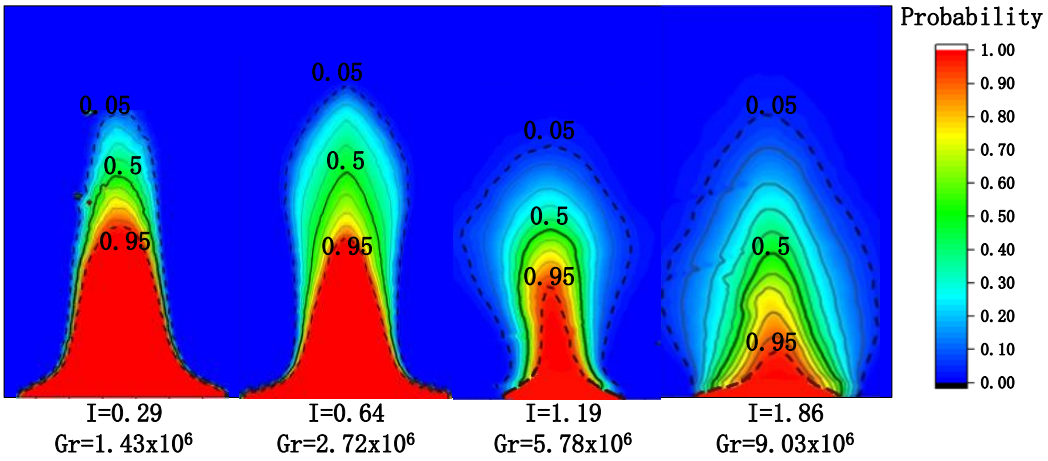

Fig. 5 (c). The oscillation intensity defined on the probability contour for pool fire with different Gr numbers.

It is interesting to observe that the separation between the 0.05 probability contour line and the 0.95 probability contour line varies significantly for different *Gr* numbers. This result indicates that the absolute separation between the contour lines can help differentiate different flame structures.

For that, the oscillation intensity is introduced and is defined as:

$$I = \frac{Area(0.05 < p < 0.95)}{2 \times Area(0.5 < p)} \tag{11}$$

where p is the probability of a pixel location. Mathematically, the numerator is the area difference in between the area associated with 0.95 probability contour line and the area associated with 0.05 probability contour line. The upper bound and low bound of the probability criteria must be unique in which the lower bound has to be larger than 0 and the upper bound has to be smaller than 1 and are selected through parametric study such that oscillation from different flame structures can be well captured. For the denominator, it describes the mean of the fluctuation and the constant is for scaling purposes. Fundamentally, the oscillation intensity is the ratio of average fluctuation to the mean if the oscillation intensity approaches 0, there is nearly no oscillation to the flame and therefore it is a laminar flame. However, flame becomes unstable and turns to turbulent when the oscillation intensity increases.

In order to verify the results obtained from this study, oscillation intensity as a function of *Gr* number obtained based on experiments carried out by of Fang et al. [15] are compared. Fig. 6 shows the two sets of data. Similar trends of oscillation intensity as a function of Gr number is observed. Using a linear fit, a power function relating the oscillation intensity and the *Gr* number is obtained and it is given as:

$$I \propto Gr^{0.98} \tag{12}$$

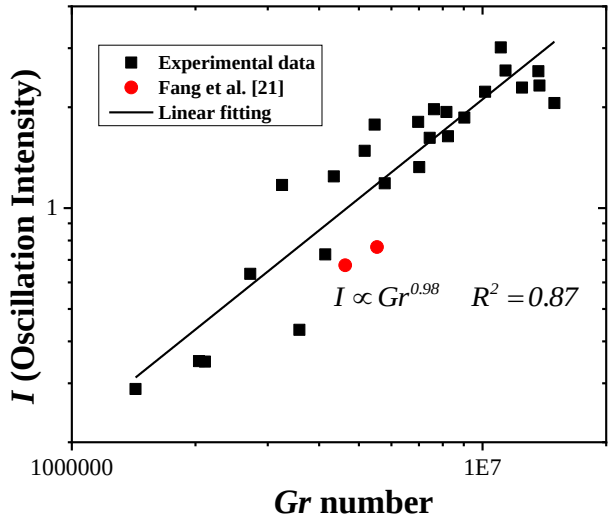

Fig. 6. Probability-based oscillation intensity with *Gr* number for pool fires with diameter ranging from 2 cm to 10 cm.

3.2 Oscillation frequency

In order to examine the time-dependent characteristic of the oscillating flame, Fast Fourier transform on pixel location with the flame envelop is conducted and the power spectral densities of the pool fire are obtained. The spectrum distributions for two different *Gr* numbers are shown in the Fig. 7. It is observed that for the pool fire with high *Gr* number, the slope of the amplitude is closer to the value of -5/3 in the high frequency region. The value of -5/3 is the characteristic value of the classical distribution in the turbulent velocity field [20] indicating that the oscillation intensity is greater for the flame with higher *Gr* number. This comparison verifies the discussion in section 3.1 where the oscillation intensity increases with *Gr* number.

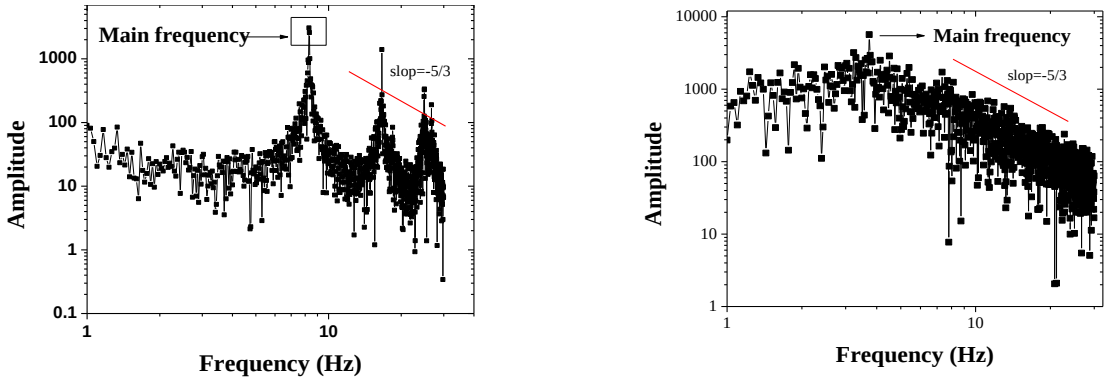

(a) Gr=4.14 X 10^6 (d=4 cm, p=150 kPa) (b) Gr=9.03 X 10^6 (d=4 cm, p=300 kPa)

Fig. 7 The power spectral densities of pool fire with different Gr number.

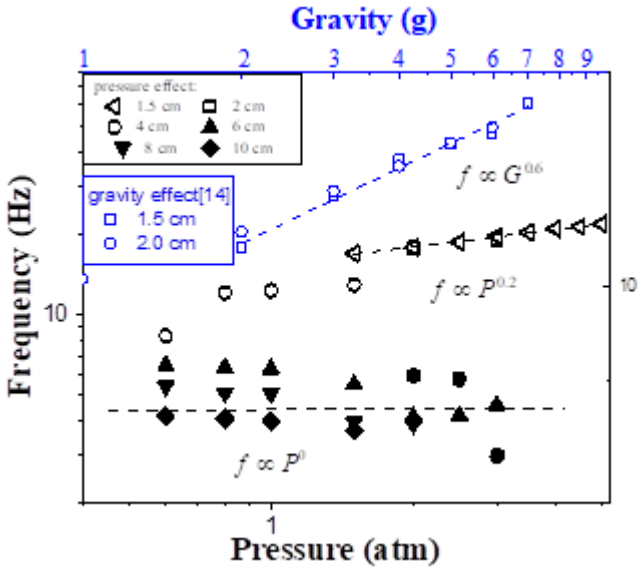

Fig. 8. The effect of different pressure and gravity conditions on frequency (hollow symbols represent tip flickering flame and solid symbols represent non- tip flickering flames).

Based on the spectrum density distribution, the frequency with the highest amplitude, namely main frequency, indicates an important parameter in pool fire oscillation. The main frequency of each test including different pressure conditions and burner diameters is shown in Fig. 8. In the same figure, previous data [8] for the main frequency of the flickering flame under different gravitation force is presented. It is shown that the influence of the pressure and the gravitation force on the main frequency depends greatly on size of the flame (due to different pool burner diameters). For the tip flickering flame obtained from [8] (blue symbols), the main frequency increases with increasing

pressure and increasing gravitational force. The main frequency is proportional to the 0.2 power and 0.6 power for pressure and gravitational force, respectively. For non-tip flickering flames, such as sinuous meandering and turbulent flame, the pressure is seemed to have negative impact to the main frequency. This observation is in agreement with the reference [21].

In order to establish the relationship between oscillation frequency and flame structure accounting for the effect of pressure, gravity, and pool fire diameter, dimensional analysis is conducted. Based on [7], the Strouhal number is defined as:

$$St = \frac{2\nu f}{gl} \tag{13}$$

where f is the dominant frequency. Based on changes in flame structure shown in Fig. 3, flame oscillation should also be related to the buoyancy instability where the upward movement of gaseous combustion products driven by buoyancy causes the generation of vortex on the flame surface [8]. For that, the motion of vortex is regarded as a one-dimensional motion along the vertical axis. The oscillation frequency assumes to be the reciprocal of the convection time which is related to the characteristic velocity of the vortex and the characteristic length of the vortex. Therefore, the dominant frequency can be approximated as:

$$f \sim 1/t_{conv} \sim v^*/l^* \tag{14}$$

As shown in Fig. 9, for the flame with a larger Gr number or pool fire with a sufficiently large diameter under normal pressure, the vortex is formed from the flame based and the characteristic length is the diameter, i.e. $l^* \sim d$. The characteristic velocity could be calculated by buoyancy induced acceleration based on $v^* \sim \sqrt{\mathrm{a}l^*}$ where a is the acceleration induced by buoyancy and is approximately equal to $\mathrm{g}\left(T_f - T_\infty / T_\infty\right)$. When the flame temperature is assumed to be constant, the characteristic velocity can be approximated as $v^* \sim \sqrt{gl^*}$. Correspondingly, the frequency can be

written as $f \sim \sqrt{g/d}$ or $f \sim \sqrt{\left(T_f - T_\infty / T_\infty\right) g/d}$. The oscillation frequency is independent of pressure condition, but as a decreasing function of increasing burner diameter (refer to Fig. 8). It should be noted the flame temperature decreases with increasing pressure due to radiation loss and consequently results in the decrease of the acceleration induced by buoyancy which leads to slight decrease in the oscillation frequency [21].

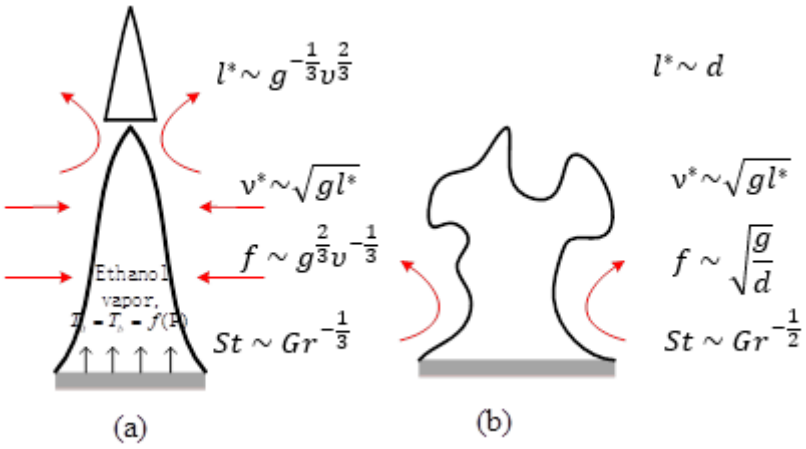

Fig. 9 Two mechanisms of flame oscillation: (a) the tip flickering flame; (b) the non-tip flickering flame.

Using the *St* number introduced in Eqn. 13, a relationship can be formed with *Gr* number. With that, a power function of $St \sim Gr^{-0.5}$ can be obtained and shown in Fig. 10. The value of the exponential component is similar to that of obtained from analysis carried out using the experimental data. For the flame with a smaller *Gr* number or pool fire with a sufficiently smaller diameter under normal pressure, the flame tip flickers while the lower flame is stable. In the study of Yuan et al. [22], this oscillating mode is modeled as a thermal plume boundary layer, and the characteristic length was obtained as $l^* \sim g^{-1/3} \upsilon^{2/3}$ by numerical solution. The characteristic velocity could be calculated by buoyancy-induced acceleration, expressed as $v^* \sim \sqrt{gl^*}$. Then, the frequency can be expressed as $f \sim g^{2/3} \upsilon^{-1/3}$ where the gas viscosity is inversely proportional to pressure and can be rewritten

as $f \sim g^{2/3} p^{1/3}$. The oscillation frequency is greatly affected by the environment where the oscillating frequency is proportional to the 1/3 power of the pressure and is proportional to the 2/3 power of gravity as approximately verified in Fig. 8. Introducing this equation into the definition of St number and Gr number, it could be obtained $St \sim Gr^{-1/3}$.

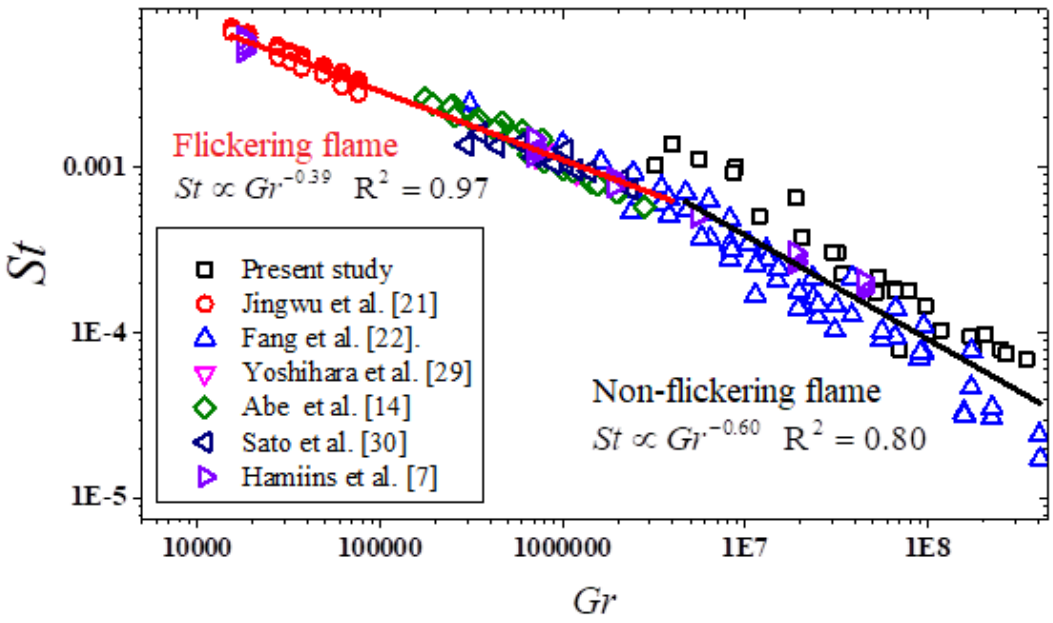

Fig. 10 Strouhal number vs. the Grashof number

As shown in the Fig. 10, the dependence of St on Gr number in current study was plotted, including other data with different diameter under different pressure conditions [15, 21], gravitational force [8, 23, 18] and fuel exit velocity [5]. It is found that correlations are successful over a range of *Gr* number (10^4 to 10^9), and there are two different relationships between the Strouhal and Froude numbers which could be explained by the two mechanisms of flame oscillation. Based on the value of *Gr* number, they are divided into flickering flame (Gr < 4 x 10^6) and non-flickering flame (Gr > 4 x 10^6), respectively. The slope of the correlation line of flickering flame is 0.39 and is larger (0.6) for non-flickering flame. The fitted values of exponent are close to the current theoretical predictions. It should be noted that the data also could be well fitted using the Strouhal–Froude number

relationship [1] where the R-square is 0.77 but it cannot distinguish the different mechanisms of flame oscillation or flame structure.

4. Conclusions

Pool fires are known to exhibit self-sustained oscillatory behavior, which plays an important role in the understanding of flame and fire spreading. The division for flame structure and the established model for flame oscillation frequency can provide a scientific prediction for the complex structure of buoyancy diffusion flame. For this reason, the ethanol pool fires with diameters from 2 cm to 10 cm were conducted under a wide range of pressure from 60 kPa to 250 kPa, where the different pressure environments were controlled using a closed high pressure chamber. The results are summarized.

(1) Based on the momentum conservation equation for the gas movement driven by buoyant force, the Gr number was derived and introduced to explain the oscillating behavior of pool fire, which coupled with the effect of ambient pressure and diameter. As the Gr number increases, the flame structure of pool fire was firstly divided in detail: laminar flame ($Gr < 1.13 \times 10^6$), tip flickering flame ($1.13\ 10^6 < Gr < 3.58 \times 10^6$), sinuous meandering flame ($3.58 \times 10^6 < Gr < 8.2 \times 10^6$) turbulent flame ($8.2 \times 10^6 < Gr$). A new mathematical methodology is developed to define the oscillation intensity of pool fire based the probability contour of flame, which provides a more accurate and objective measurement from the recorded flame video. Furthermore, the oscillation intensity of pool fire increases with the Gr number and could be fitted as $I \propto Gr^{0.98}$ using data measured in our study and previous study.

(2) The influence of ambient pressure and gravity on oscillation frequency depends on the flame oscillation mechanisms, the tip flickering flame or the non-tip flickering flame. The changes of frequency for two types of oscillation are explained and compared with experimental results, where the flame oscillation is modeled as the one-dimensional movement of vortex along the axis. For the

tip flickering flame, the oscillating frequency is proportional to the 1/3 power of the pressure and is proportional to the 2/3 power of gravity, and the relationship of dimensionless numbers can be expressed as $St \sim Gr^{-1/3}$. For non- tip flickering flame, the oscillation frequency is independent of ambient pressure and decreases with increasing diameter, and it was obtained as $St \sim Gr^{-0.5}$. It should be noted that the data also could be well fitted using the classical relationship i.e. the Strouhal –Froude number relationship, but it cannot distinguish the different mechanisms of flame oscillation.

Acknowledgements

This work, excluding Wai Cheong Tam, Wei Tang, and Chao Zhang, was supported by the National Key R&D Program of China [No.2016YFC0802101]. The authors are very grateful to Anthony Hamins from NIST for his valuable discussions of this paper.

References

[1] Hamins A, Yang J, Kashiwagi T. An experimental investigation of the pulsation frequency of flames. Proc Combust Inst 1992;24:1695-702.

[2] Cetegen BM, Ahmed TA. Experiments on the periodic instability of buoyant plumes and pool fires. Combust Flame 1993;93(1-2):157-84.

[3] Ding Y, Wang C, Lu S. The effect of azeotropism on combustion characteristics of blended fuel pool fire. J Hazard Mater 2014;271:82-8.

[4] Chen J, Bao QJPE. Digital image processing based fire flame color and oscillation frequency analysis. Procedia Eng 2012;45:595-601.

[5] Emori R, Saito K. A study of scaling laws in pool and crib fires. Combust Sci Technol 1983;31(5-6):217-31.

[6] Beji T, Merci B. Blind simulation of periodic pressure and burning rate instabilities in the event

of a pool fire in a confined and mechanically ventilated compartment. Combust Sci Technol 2016;188(4-5):504-9.

[7] Moreno-Boza D, Coenen W, Carpio J, Sánchez AL, Williams FA. On the critical conditions for pool-fire puffing. Combust Flame 2018;192:426-38.

[8] Abe H, Ito A, Torikai H. Effect of gravity on puffing phenomenon of liquid pool fires. Proc Combust Inst 2015;35(3):2581-7.

[9] Durox D, Yuan T, Villermaux E. The effect of buoyancy on flickering in diffusion flames. Combust Sci Technol 1997;124(1-6):277-94.

[10] Chen J, Zhao Y, Chen X, Li C, Lu S. Effect of Pressure on the Heat Transfer and Flame Characteristics of Small-Scale Ethanol Pool Fires. Fire Saf J 2018.

[11] Zhang J, Lu S, Li Q, Yuen RKK, Chen B, Yuan M, et al. Smoke filling in closed compartments with elevated fire sources. Fire Saf J 2012;54:14-23.

[12] Wang Z, Tam WC, Chen J, Lee KY, Hamins A. Thin Filament Pyrometry Field Measurements in a Medium-Scale Pool Fire. Fire Technol 2020;56(2):837-61.

[13] Ditch BD, de Ris JL, Blanchat TK, Chaos M, Bill Jr RG, Dorofeev SB. Pool fires–An empirical correlation. Combust Flame 2013;160(12):2964-74.

[14] Chen J, Zhang X, Zhao Y, Bi Y, Li C, Lu S. Oxygen concentration effects on the burning behavior of small scale pool fires. Fuel 2019;247:378-85.

[15] Wang J, Fang J, Guan J, Zeng Y, Zhang Y. Flame volume and radiant fraction of jet diffusion methane flame at sub-atmospheric pressures. Fuel 2016;167:82-8.

[16] Fang J, Wang J, Guan J, Zhang Y, Wang J. Momentum- and buoyancy-driven laminar methane diffusion flame shapes and radiation characteristics at sub-atmospheric pressures. Fuel 2016;163:295-303.

[17] Incropera FP, Lavine AS, Bergman TL, DeWitt DP. Fundamentals of heat and mass transfer. Wiley; 2007.

[18] Quintiere J. Fundamentals of fire phenomena. Wiley; 2006.

[19] Yan WG, Wang CJ, Guo J. One extended OTSU flame image recognition method using RGBL and stripe segmentation. Appl Mech Mater 2012;121:2141-5.

[20] Weckman E, Strong A. Experimental investigation of the turbulence structure of medium-scale methanol pool fires. Combust Flame 1996;105(3):245-66.

[21] Fang J, Tu R, Guan J, Wang J, Zhang Y. Influence of low air pressure on combustion characteristics and flame pulsation frequency of pool fires. Fuel 2011;90(8):2760-6.

[22] Yuan T, Durox D, Villermaux E. An analogue study for flame flickering. Exp Fluids 1994;17(5):337-49.

[23] Yoshihara N, Ito A, Torikai H. Flame characteristics of small-scale pool fires under low gravity environments. Proc Combust Inst 2013;34(2):2599-606.

[24] Sato H, Amagai K, Arai M. Scale modeling of puffing frequencies in pool fires related with Froude number. Progress in Scale Modeling 2008. 133-47.

[25] Wheeler AJ, Ganji AR. Introduction to engineering experimentation. Prentice Hall New Jersey; 1996.

[26] Ji J, Gong C, Wan H, Gao Z, Ding L. Prediction of thermal radiation received by vertical targets based on two-dimensional flame shape from rectangular n-heptane pool fires with different aspect ratios. Energy 2019;185:644-52.

[27] Wan H, Gao Z, Ji J, Zhang Y. Experimental study on flame radiant heat flux from two heptane storage pools and its application to estimating safety distance. Energy 2019; 82:11-20.

Appendix A. Uncertainty analysis

The uncertainty analysis for the flame oscillation measurement is used by the method of Wheeler and Ganji [25], which is widely recognized for calculating the uncertainty of pool fire characteristic parameters [26, 27].

In our study, the Gr number was obtained by the measured variables in the experiment, such as the mass loss rate, ambient pressure, ambient temperature. The Gr number was expressed as

$$\mathrm{Gr} = func(P^2, T^{-2}, \dot{m}^{6/5})$$

Based on the method of Wheeler and Ganji [25], the relative uncertainty of Gr number is written as

$$\frac{\delta Gr}{\mathrm{Gr}} = \left[\left(2\frac{\delta P}{P} \right)^2 + \left(2\frac{\delta T}{T} \right)^2 + \left(6/5\frac{\delta \dot{m}}{\dot{m}} \right)^2 \right]$$

where $\delta P, \delta T, \delta \dot{m}$ are relative uncertainties of the measured pressure, the measured temperature and the measured mass loss rate, respectively.

Considering the repeatability error and reading precision error, relative uncertainties of the measured pressure, the measured temperature and the measured mass loss rate were estimated as 5%, 8% and 7%, respectively. Then, the relative uncertainty of Gr number was calculated as 21%. Based on the similar method, the relative uncertainty of St number ($St = \frac{2\nu f}{gl}$) was calculated as 5%. Otherwise, the total uncertainty of flame oscillation intensity was mainly caused by the repeatability error and the measuring error due to the image processing method, of which the uncertainty is 5.0%, 6.0%, respectively. The relative uncertainty of flame oscillation intensity was calculated as 12%.